The International Journal of Advanced Manufacturing Technology (2019) 102:685–694
https://doi.org/10.1007/s00170-018-03209-5

ORIGINAL ARTICLE

Isothermal closed-die forming process of magnesium alloy upper receiver: numerical simulation and experiments

Qiang Chen[1] · Xiaohua Zhang[2] · Jun Lin[1] · Hong Zhan[1] · Zude Zhao[1] · Zhiwen Xie[3] · Baoguo Yuan[4]

Received: 22 July 2018 / Accepted: 17 September 2018 / Published online: 5 January 2019

Abstract
An isothermal closed-die forming process, including two forging procedures in which the female die of the final forging procedure is split into two parts, was developed, and a very complex component of magnesium alloy called the upper receiver was successfully produced. The obtained forged piece has higher mechanical properties and meets the standard of being safely used in special machines. Based on the FORGE software platform, finite element (FE) simulation was used to determine the preform shape, processing parameters, and forging procedure. A closed-die cavity was formed during the final forging procedure, which can effectively enhance the workability of magnesium alloy, refine the grain sizes, and increase the strength of the component. Importantly, the forged piece has homogeneous microstructures, and the ultimate tensile strength located at the lateral and bottom positions of the upper receiver is greater than 396 MPa and the minimum of the elongation ratio at fracture is 15%.

Keywords Closed-die forming process · Magnesium alloys · Finite element simulation · Upper receiver

1 Introduction

There has been increasing application of magnesium alloys for lightweight structural components in the automotive and aerospace industries because of their high specific strength, outstanding machinability, good damping capacity, and low density [1, 2]. At present, a great number of magnesium alloy parts are produced by the casting process. However, magnesium alloy products treated by die casting exhibit low mechanical properties due to casting defects, such as gas porosity, needle holes, and cold shut.

The hot forging process can improve the poor workability of magnesium alloys caused by their close-packed hexagonal (HCP) crystal structure, and enhance the mechanical properties of the products as well. Therefore, some researchers focused on investigating the forging technology of magnesium alloys. Lim et al. [3] investigated the plane-strain forging of AZ31wrought magnesium alloy. Skubisz et al. [4] studied the forgeability of AZ31/AZ61 magnesium alloys in hot and warm closed-die forging. Li et al. [5–7] researched the microstructure characteristics and deformation behavior of AZ31 magnesium alloy by means of different methods, including alternate forward extrusion and continuous variable cross-section direct extrusion (CVCDE). Ogawa et al. [8] assessed the forming limit of magnesium alloy at elevated temperatures for precision forging and drew the conclusions that Mg alloy shows an excellent workability at temperatures from 250 to 400 °C, and temperatures higher than 400 °C are not suitable for the forming of Mg alloy because of heavy oxidation. Hsiang et al. [9] predicted the mechanical properties and forming loads in terms of AZ31 and AZ61 magnesium alloys during hot extrusion by applying the artificial neural networks (ANN) analysis method, and the optimal processing parameters with a determined extrusion ratio were accurately

✉ Xiaohua Zhang
zxhhrbu@hrbust.edu.cn

✉ Jun Lin
cqlinjun@126.com

[1] Southwest Technology and Engineering Research Institute, 400039 Chongqing, People's Republic of China

[2] School of Materials Science and Engineering, Harbin University of Science and Technology, 150040 Harbin, People's Republic of China

[3] University of Science and Technology Liaoning, 114051 Anshan, People's Republic of China

[4] School of Materials Science and Engineering, Hefei University of Technology, 230009 Hefei, People's Republic of China

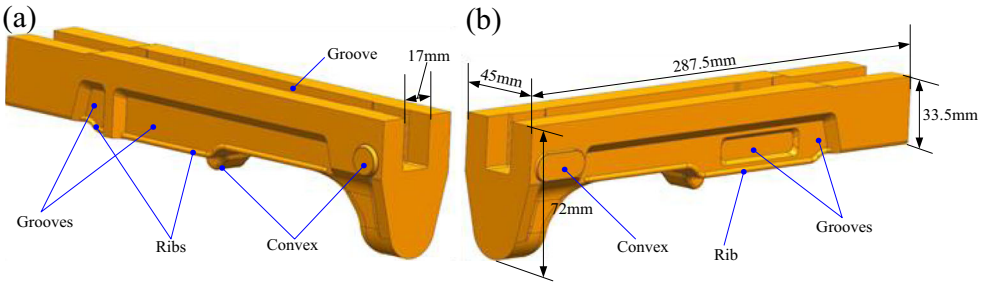

Fig. 1 The shape and typical dimensions of the upper receiver: **a** left face and **b** right face

obtained. Li et al. [10] investigated the effects of the newly proposed multidirectional forging (MDF) process with an increased strain rate on the microstructure and mechanical properties of AZ61 magnesium alloy. Kuo et al. [11] reported the springback of L-bending for AZ31 magnesium alloy sheets at different temperatures by means of the Taguchi method. Li et al. [12] designed a one-pass hot spinning process of AZ31 magnesium alloy sheet and investigated the effects of the process parameters on the quality of the formed workpiece. Wang et al. [13] proposed a new concept of the hollow billet to decrease the forming load for the hot precision forging of an AZ80 magnesium alloy wheel. Karparvarfard et al. [14] conducted the microstructure, texture, and mechanical behavior characterization of hot forged cast ZK60 magnesium alloy. Liu et al. [15] proposed the two-stage hot forming process of an AZ31B spur bevel gear by combining experiments with the finite element method (FEM). Based on the finite element simulation and experimental methods, Hwang et al. [16] revealed the mechanical properties of the extruded seamless AZ61 magnesium alloy tube products with and without reinforced silicon carbide particulates (SiCp). Xia et al. [17] investigated the isothermal forging of a cast Mg–Zn–Y–Zr magnesium alloy tank cover by using finite element simulations and experiments and found that the mechanical properties of the tank cover when utilizing the optimum isothermal forging process show a significant improvement over those of original materials. Shan et al. [18] studied the isothermal precision forging process of Mg-10Gd-2Y-0.5Zn-0.3Zr alloy, and they developed a combined female die composed of five parts to successfully produce a bracket with a height to width ratio of 9.5. Cai et al. [19] developed a multi-stage variable speed (MSV) isothermal forming process based on strain rate sensitivity (SRS) analysis and made a conclusion that grain refinement can be obtained by utilizing the developed isothermal forming process with severe plastic deformation to improve the mechanical properties of Mg products. Yuan et al. [20] reported on the isothermal forging process of a large-sized AZ80 magnesium alloy forging by means of finite element simulation combined with experiments. Lin et al. [21] studied the influence of plastic anisotropy on the deep drawing formability of a ZK60 magnesium alloy sheet with experimental and simulative methods. Shan et al. [22] studied the precision forging technology for a complex-shaped magnesium alloy forging by adopting a scheme of isothermal forming and the use of a female die. He et al. [23] studied the isothermal forging of a large AZ80 magnesium alloy support beam with a projective area of 0.22 m^2.

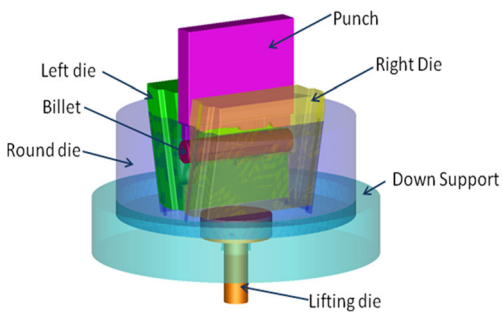

Fig. 2 Schematic model for the final forging operation

From the literature review mentioned above, we can find that only limited work has been reported on the hot closed-die precision forging of magnesium alloys. In the present work, the workability of AZ80 magnesium alloy was first investigated and the constitutive model of the alloy was established. Then, the two-stage hot precision forming process with a closed-die cavity was developed. Moreover, the processing parameters were optimized by an FE simulation. According to the numerical simulation results, the hot precision die forging experiments of an AZ80 magnesium alloy upper receiver were successfully conducted.

2 Forging process design of the upper receiver component

The upper receiver component's outline dimensions are 287.5 mm × 45 mm × 72 mm. Its characteristic shape is that the dimension in the long direction is greater than those in the breadth and height directions, and there are ribs, grooves, and convexes in the top, down, left, and right faces (Fig. 1). The material of the upper receiver is extruded AZ80 magnesium alloy, which is a hard forming material.

No matter which forging process is used to form the upper receiver, the female die in the final forging procedure should be split into two parts in order to form the ribs, convexes, and grooves, as drawn in Fig. 2. Due to the complexity of the structure, it was very difficult to ensure full-

Table 1 Summarized extended Sellars-Tegart-Garofalo models

Types	Equations and values of parameters
Flow stress $\sigma < \sigma_{\text{critical}}$	$\sigma = \frac{\mu}{\mathrm{A}} \cdot \varepsilon$
	Here, $\mu = 16440 \cdot \left(1 - 0.29 \cdot \frac{T}{405+273.15}\right)^{2.51}$; $\mathrm{A} = 66.2578 \cdot Z^{-0.0486}$
Flow stress $\sigma \geq \sigma_{critical}$	$\frac{d\sigma}{d\varepsilon} = \frac{d\sigma_{\varepsilon}}{d\varepsilon} - \Delta\sigma \cdot \frac{\ln(2)}{\dot{\varepsilon} \cdot t_{50}^{n_{Av}}} \cdot n_{Av} \cdot (1 - X_v) \cdot \left[\frac{-t_{50}^{n_{Av}} \cdot \ln(1-X_v)}{\ln(2)}\right]^{1-\frac{1}{n_{Av}}}$;
	$\frac{d\sigma_{\varepsilon}}{d\varepsilon} = \frac{E}{\mu} \cdot \left(1 - \left(\frac{\sigma_{\varepsilon} - \sigma_{yield} + X_v \cdot \Delta\sigma}{\sigma_{\text{saturation}} - \sigma_{yield}}\right)^2\right) \cdot \frac{\sigma_{\text{saturation}} - \sigma_{yield}}{\sigma_{\varepsilon} - \sigma_{yield}}$;
	$X_v = (\sigma_{\varepsilon} - \sigma) \cdot \Delta\sigma^{-1}$; $\Delta\sigma = \sigma_{\text{saturation}} - \sigma_{\text{steady}}$
	Here, $t_{50} = 0.011 \cdot Z^{-0.877} \cdot \exp\frac{Q}{R \cdot T}$; $n_{Av} = 2.891$;
	$\sigma_{\text{yield}} = 73.52 \cdot \text{asinh}\left(\frac{Z}{2.187 \times 10^9}\right)^{\frac{1}{5.657}} + 5.66$; $\sigma_{\text{critical}} = 66.86 \cdot \text{asinh}\left(\frac{Z}{1.659 \times 10^9}\right)^{\frac{1}{4.468}}$;
	$\sigma_{\text{steady}} = 109.10 \cdot \text{asinh}\left(\frac{Z}{3.136 \times 10^9}\right)^{\frac{1}{4.305}}$; $\sigma_{\text{saturation}} = 128.45 \cdot \text{asinh}\left(\frac{Z}{3.091 \times 10^9}\right)^{\frac{1}{4.029}} + 3.98$
Zener–Hollomon parameters	$Z = \frac{\dot{\varepsilon}}{\dot{\varepsilon}_0} \cdot \exp\frac{\mathrm{Q}}{\mathrm{R} \cdot \mathrm{T}}$; $\dot{\varepsilon}_0 = 1 s^{-1}$; $\mathrm{Q} = 127077 \mathrm{J} \cdot \mathrm{mol}^{-1}$; $\mathrm{R} = 8.314 \mathrm{J} \cdot \mathrm{mol}^{-1} \cdot \mathrm{K}^{-1}$

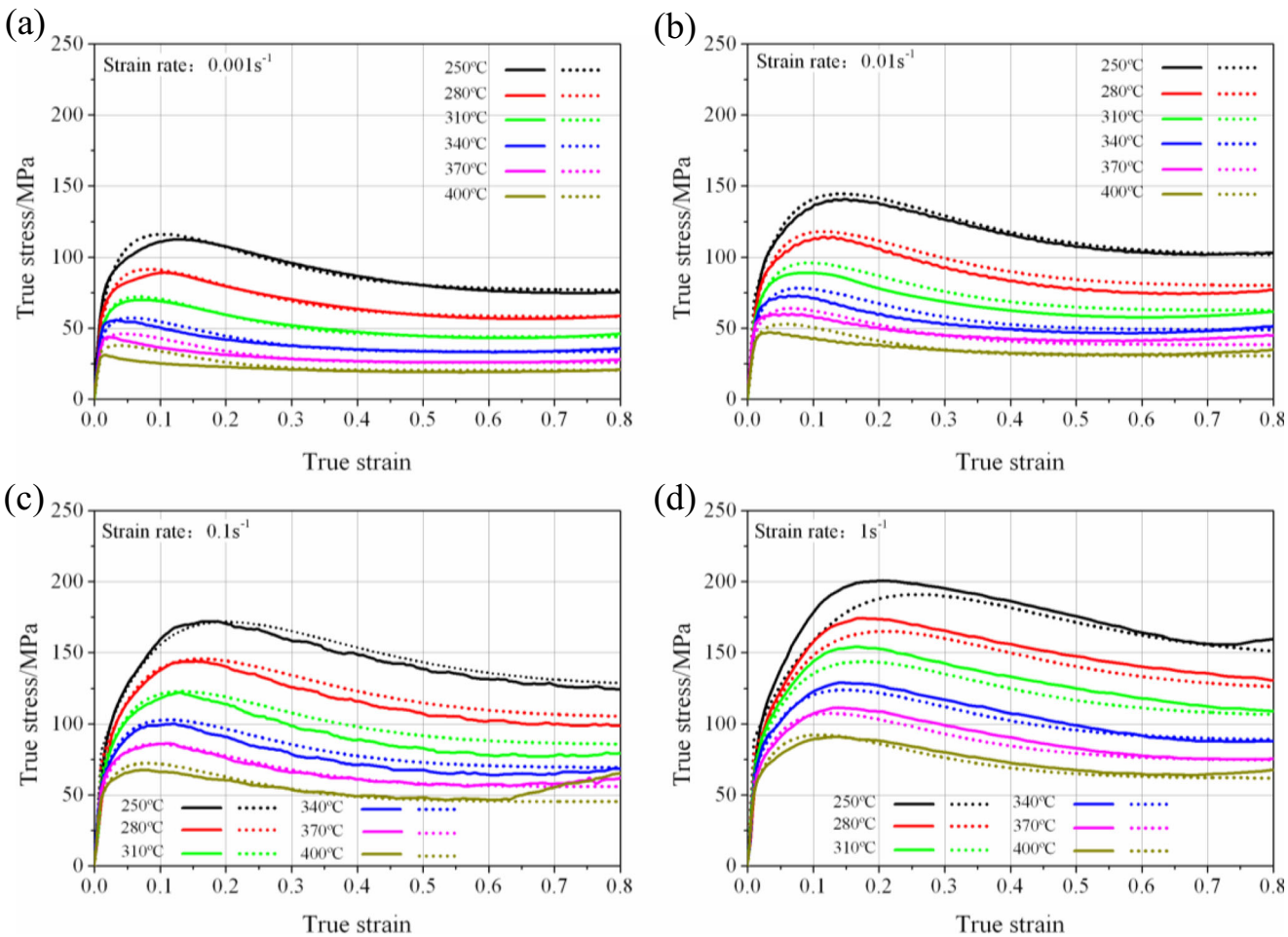

Fig. 3 Comparison between the calculation and experimental results under different strain rates: **a** 0.001 s^{-1}. **b** 0.01 s^{-1}, **c** 0.1 s^{-1}, and **d** 1 s^{-1}

Table 2 Thermo-physical parameters of AZ80 magnesium alloy

Properties	Values
Thermal conductivity (W/(m°C))	58.5 (20 °C), 69.3 (200 °C), 75.2 (350 °C)
Specific heat (kJ/(kg°C))	1.129 (20 °C), 1.255 (200 °C), 1.297 (350 °C)
Linear expansion coefficient (1/°C)	2.9×10^{-5}
Density(g/cm^3)	1.94

filling in the forging procedure when using conventional measures. Therefore, the isothermal forging process is suitable to form such a complex component. Moreover, since the product works under complex impact loading, it needs to have a fine-grained microstructure to obtain enough strength to guarantee pressure resistance. As seen from Fig. 2, the final forging process is a closed-die forming one which improves the filling ability and grain refinement because the die structure would form one state of triaxial compressive stress.

3 FE simulation model

It is costly in finance and time to use the classical "Trial and Error" method to design the shape of the billet or to preform and optimize the processing parameters. The FE method is employed to assist in the design of the forming process of the upper receiver forging. The FORGE software is employed for the simulation of the isothermal forging conducted in the present study.

To build an accurate simulation model, the true stress-strain relations of extruded AZ80 magnesium alloy were obtained by an isothermal compression test at the temperatures ranging from 250 to 400 °C with strain rates ranging from 0.001 to 1 s^{-1} by using a 3500-Gleeble thermal simulator. Based on extended Sellars-Tegart-Garofalo relationships [24, 25], the constitutive model of AZ80 has been established (Table 1).

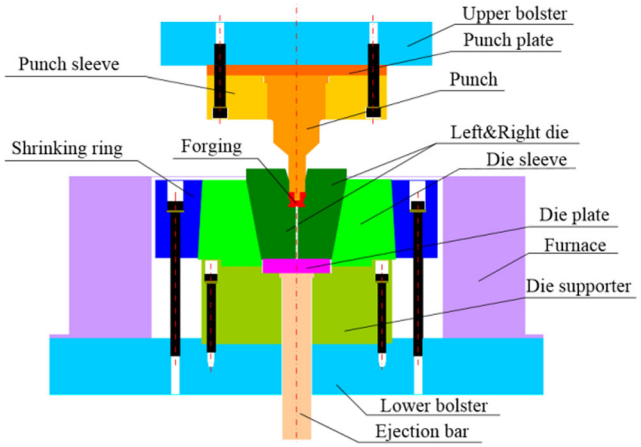

Fig. 5 Schematic of the die system for the final forging forming process

Figure 3 presents the comparison between the calculation and experimental results under different strain rates, in which the solid line represents the experimental result and the dotted line stands for the calculation one. As a result, the error between the experimental and calculation curves is less than 5%. The constitutive model has been embedded in the software of FORGE through secondary development using the Fortran language. Other thermo-physical parameters of the AZ80 used in the simulation model are given in Table 2.

Since the split female dies would be passively moved into the round die during the forming procedure (Fig. 2), both split dies should be defined as elastic material in the simulation model according to the requirement. H13 hot die steel would be used as the punch and split dies material. The Young's modulus of the female dies, the coefficient of Poisson, the density, the thermal conductivity, and the specific heat are 200 GPa, 0.30, 7850 kg/m^3, 35.5 W/(m°C), and 7.78 kJ/(kg°C), respectively. All other dies, including the punch, would be set as rigid material in the simulation model.

In this study, a hydraulic pressure machine with a capacity of 8000 kN was employed, allowing for the maximum loading force of 7200 kN due to safety consideration. The velocity of the upper beam of the machine is set as 16 mm/s.

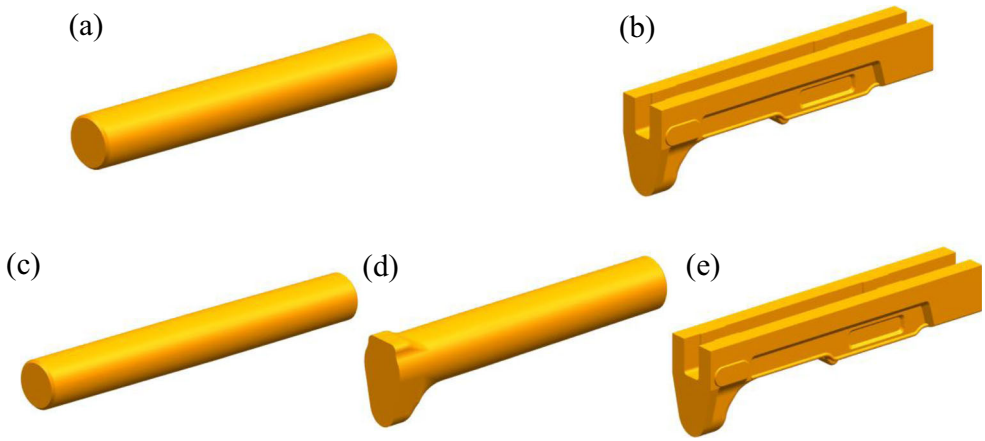

Fig. 4 Schematic of two forming processes of the upper receiver: **a** cylindrical bar for the first forming process, **b** final forged piece for the first forming process, **c** cylindrical bar for the second forming process, **d** preform for the second forming process, and **e** final forged piece for the second forming process

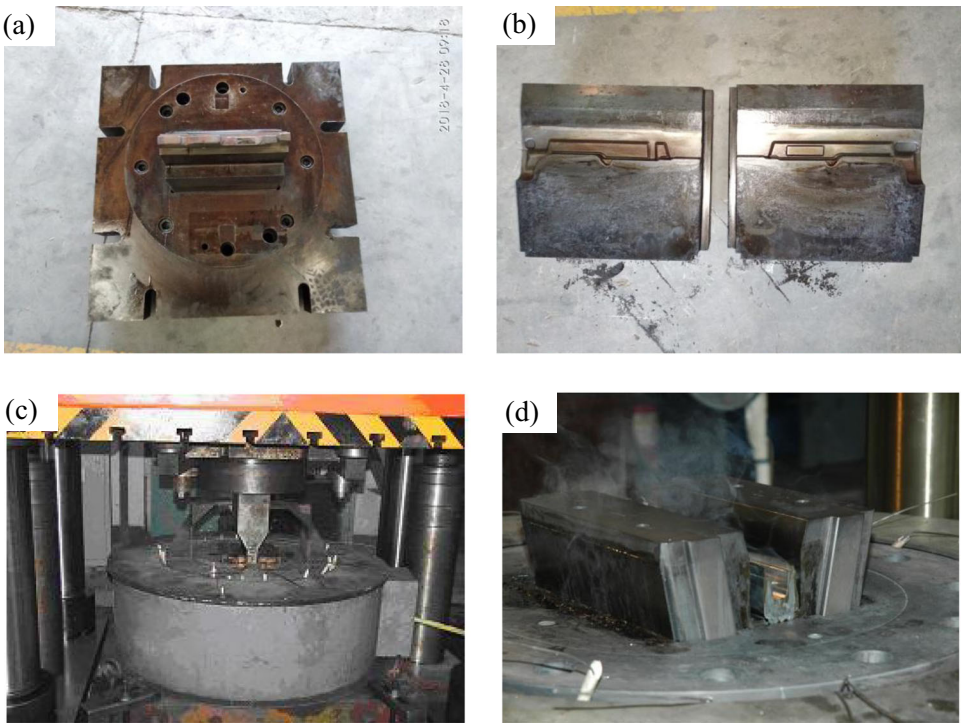

Fig. 6 Experimental set-up for the upper receiver component: **a** punch, **b** female dies, **c** final forging die system, and **d** experimental work

The heat exchange coefficient between the workpiece and the environment is 18 W/m^2/°C, and the one between the workpiece and dies is 10 KW/m^2/°C. The friction model was assumed to follow the shear friction mode:

$$f_f = \begin{cases} \mu \cdot \sigma_n & if\ \sigma_n < \left(\sigma_0/\sqrt{3}\right) \\ \mu \cdot \left(\sigma_0/\sqrt{3}\right) & if\ \sigma_n \geq \left(\sigma_0/\sqrt{3}\right) \end{cases} \quad (1)$$

where μ is the friction factor, σ_n is the normal stress, and σ_0 is the flow or yield stress. The constant friction coefficient between the workpiece and split female dies is determined to be 0.08 [26], and the coefficient between split female dies and the round die is 0.15 [27].

The isothermal forging process is determined to be employed in this paper due to the material characteristics of magnesium alloy. In the processing experiments, the workpiece temperature is nearly equal to the temperature of female dies, but the punch one is often 30 °C lower than that of the female die. For example, if the workpiece temperature was 350 °C, the punch temperature is only 320 °C, but the temperatures of the other dies are 350 °C. Therefore, these should be taken into account in the simulation models.

In this study, two different isothermal precision forming processes for the AZ80 upper receiver forging were designed. The first forming process uses a cylindrical bar as the billet which is directly forged into the final forged piece (Fig. 4a, b).

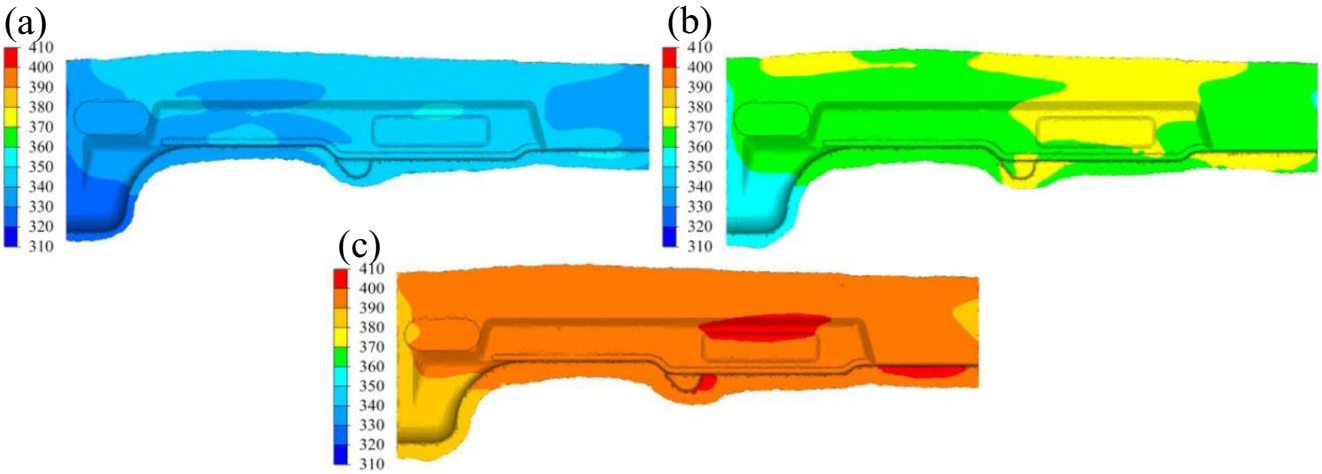

Fig. 7 Temperature distributions of the final forged piece obtained by simulation: **a** initial temperature of 320 °C, **b** initial temperature of 350 °C, and **c** initial temperture of 380 °C

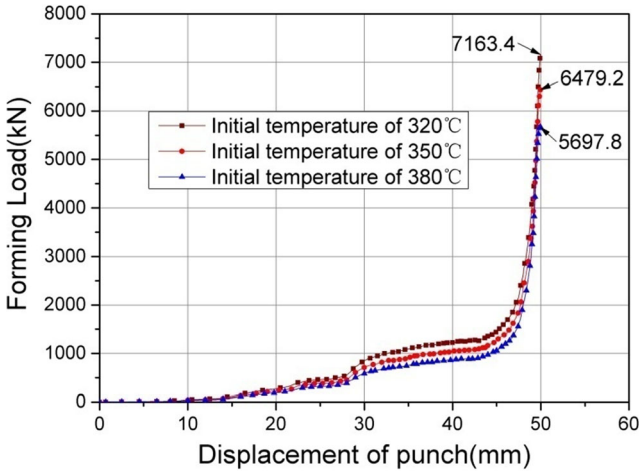

Fig. 8 Forming loads of different initial temperatures

The second forming process is based on the principle that the cross-sectional area of the preform is almost equal to that of the final forged piece, and the ratio of the cross-sectional area of the preform and the final forged piece ranges from 0.90 to 1.10. Therefore, the second forming process includes two forging stages and the evolution of the workpiece is shown in Fig. 4c–e.

4 Experimental procedures

The billet used in the first forging forming process is an AZ80 magnesium alloy cylinder bar with a diameter of 40.5 mm and a length of 287 mm, and the dimension of the billet used in the second forging forming process is Φ39.5 mm × 299 mm.

A detailed description of the final die structure is drawn in Fig. 5. The punch and female dies used in the experimental work are shown in Fig. 6a, b, respectively. The photograph of the final dies and the experimental work are shown in Fig. 6c, d, respectively. The forming speed of the upper receiver is set as 16 mm/s, which is equal to the punch speed used in the FE model.

After forging, the forged pieces were cooled to room temperature in the air. Samples for the optical microscope (OM) were cut from the different regions of the forged piece. After mechanically polishing and etching with picric acid, the samples were examined using an Olympus OM. After an aging treatment (180 °C × 8 h), the tensile samples, which were cut from the forged piece, were machined and the tensile test was carried out under room temperature with an initial strain rate of 0.01 s^{-1} using an Instron-5500 electronic testing machine and was repeated three times.

5 Results and discussion

5.1 Effect of initial temperature on the forming procedure

Taking the second forging forming process as the research object, three temperature parameters of 320, 350, and 380 °C for the workpiece were designed, which were used in the simulation experiment. The temperature distributions of the final forged piece, as calculated by the FE simulation software, are shown in Fig. 7. When the temperature of the workpiece was set as 380 °C, the temperature of the final forging is greater than 400 °C (Fig. 7c). For magnesium alloy, however, a higher temperature remarkably decreases the mechanical properties of the final forgings, and thus, the initial temperatures should be lower than 380 °C. The forming loads

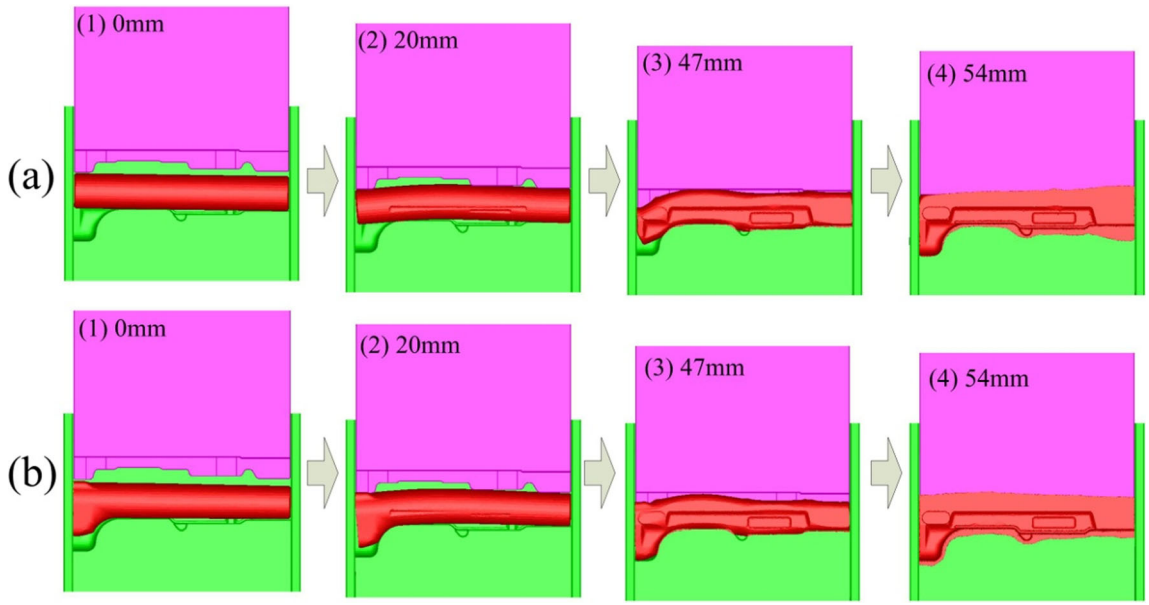

Fig. 9 Evolution of different workpiece shapes at many typical punch displacement values: **a** first forging process and **b** second forging process

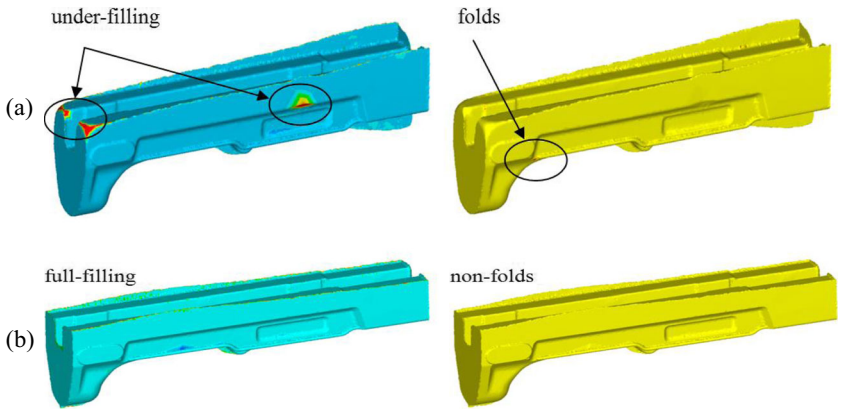

Fig. 10 Forming defects of the two forging processes (red zones stand for forming defects): **a** first forging process and **b** second forging process

calculated by the FE simulation are drawn in Fig. 8. Taking the allowable load force of the machine into account, the initial temperature of the workpiece would be set as 350 °C in the following studies.

5.2 Effect of workpiece shape on the final forging procedure

To analyze the material flow of the workpiece in the final forging procedure, two designed processes (Fig. 4) were employed with the same parameters, and here the workpiece temperature was 350 °C. Figure 9 shows the shape evolutions of the two forging processes at different stroke distances. When the punch moved downwards from 0 to 20 mm, there was no obvious difference between the two processes. The billets were only subjected to bending deformation and the metals were forced to flow into the cavity of the head part. When the stroke increased to 47 mm, the metal flow in the second forging forming process became much easier compared to the first forming process, but in the first forming process, the end part almost had been overflowed. With the punch displacement increasing to 54 mm, the filling effect of the first forming process was far worse because the flow resistance was increased far more, and excess flash was formed at the end part. Therefore, it was easy to generate several defections, such as under-filling and folds (Fig. 10a). Nevertheless, these defections can be avoided successfully by using the second forming process (Fig. 10b).

Figure 11a shows the experimental photographs of the upper receiver forging treated by the first forging process after removing the flash. Under-filling located at the head end can be found in the first forging process, which is in good agreement with the simulation results. Figure 11b, c shows the photographs of the preform and final forgings of the upper receiver treated by the second forging process after removing the flash. The preform and final forging of the upper receiver are shown to be good, and no problems can be discovered by the second forging process. Moreover, the surfaces are smooth without any defects in the metal filling and fold. The first reason is that hot forging can effectively eliminate the die-

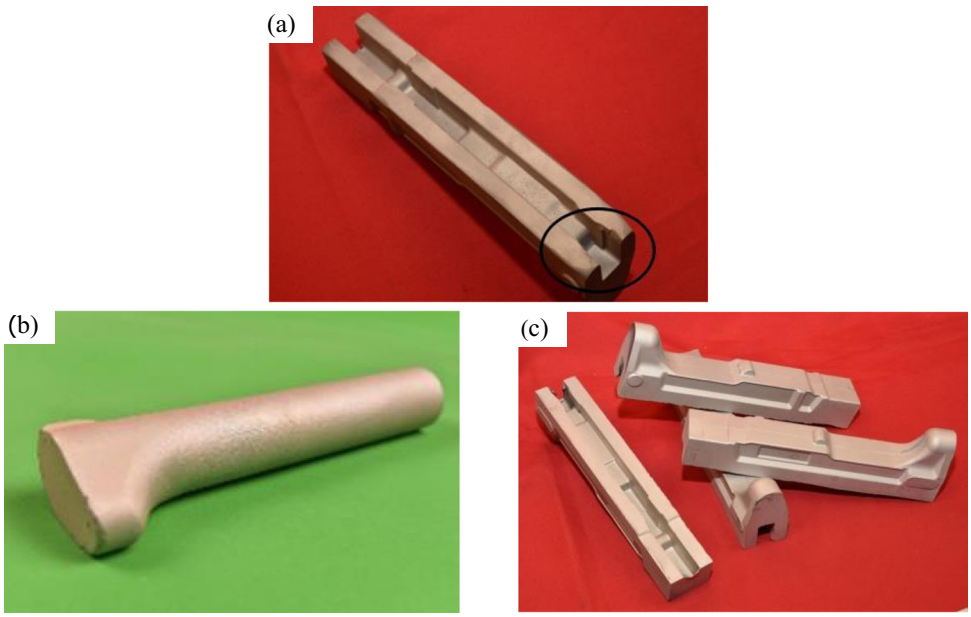

Fig. 11 Photographs of the upper receiver obtained by different processes after removing flash: **a** forged piece obtained by the first forging process, **b** preform workpiece obtained by the second forging process, and **c** forged piece obtained by the second forging process

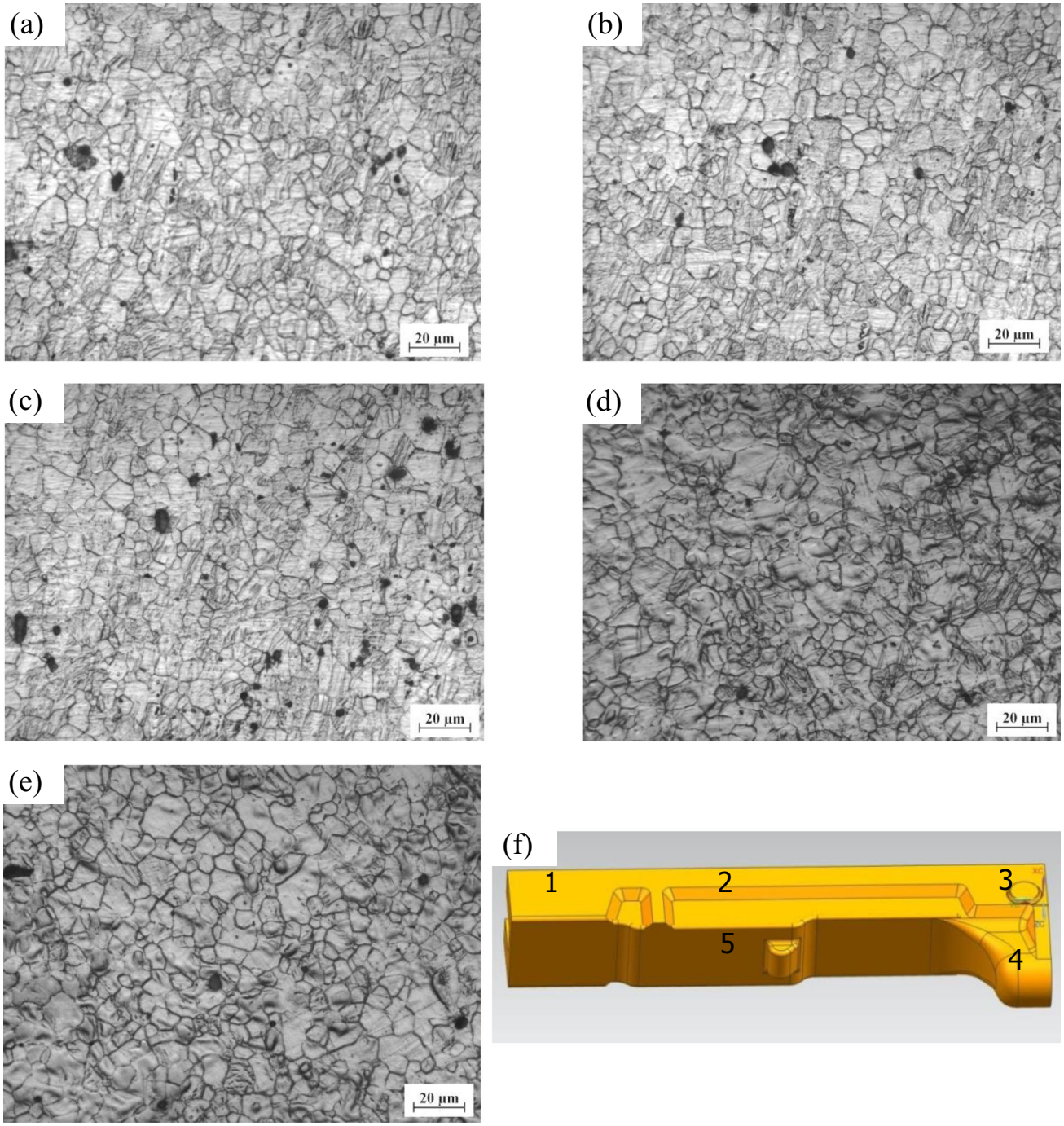

Fig. 12 Microstructures of upper receiver forging located at different positions: **a** position 1, **b** position 2, **c** position 3, **d** position 4, **e** position 5, and **f** sketch of sample locations

chilling effect and improve the workability and die filling of magnesium alloys. In general, the formability of magnesium alloys is relatively poor compared to aluminum alloys due to their limited number of slip systems that originated from their HCP crystal structure. The second reason is that the preform design based on the constant cross-sectional area plays a significant part in the improvement of the quality of finished forgings. The gathering materials of the preform design, to some extent, effectively reduce the uneven deformation, decrease the resistance of the deformation and promote sufficient filling in the stage of the final forging operation. The third reason is that the billet is under triaxial compressive stress, which affords the billet outstanding plasticity and prevents the cracking phenomena from happening, although the forming speed is relatively high. Therefore, the second forming process was employed in the following study.

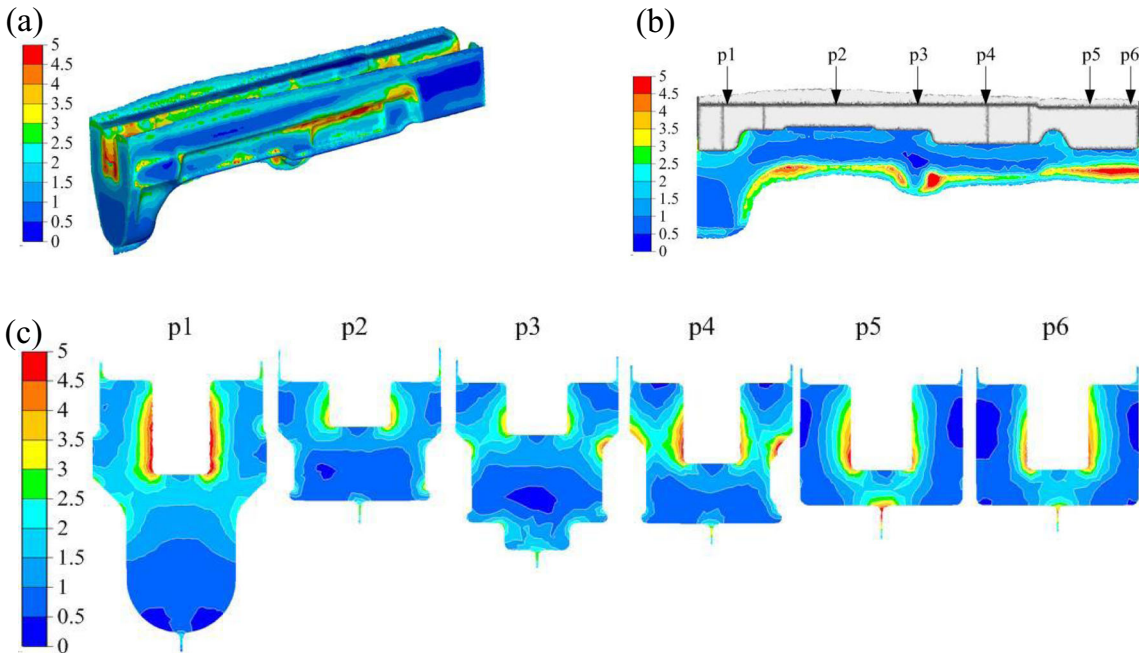

Fig. 13 Distribution of equivalent strain after the final forging process: **a** global distribution, **b** distribution on the axial-direction cut plane, and **c** distributions on the cut planes of the typical points

5.3 Microstructure analysis and mechanical properties

Figure 12 shows the microstructures of the upper receiver forging located at different positions. As shown in Fig. 12, the mean grain sizes located at positions 1, 2, 3, 4, and 5 are 13, 14, 13, 18, and 17 μm, respectively. It is generally accepted that dynamic recrystallization occurs during hot deformation for magnesium alloys. The main reason can be attributed to limited slip systems, relatively low stacking fault energy, and a high rate of grain boundary diffusion for magnesium alloys. Note that the mean grain sizes located at positions 4 and 5 are slightly greater than those located at positions 1, 2, and 3.There are two main reasons. First, metals located at position 4 are subjected to enough deformation in the perform stage. However, rapid grain coarsening at position 4 cannot be avoided due to finer grains and higher interfacial energy during heat preservation for final forging. Moreover, the metals located at position 4 cannot obtain enough deformation in the stage of final forging.

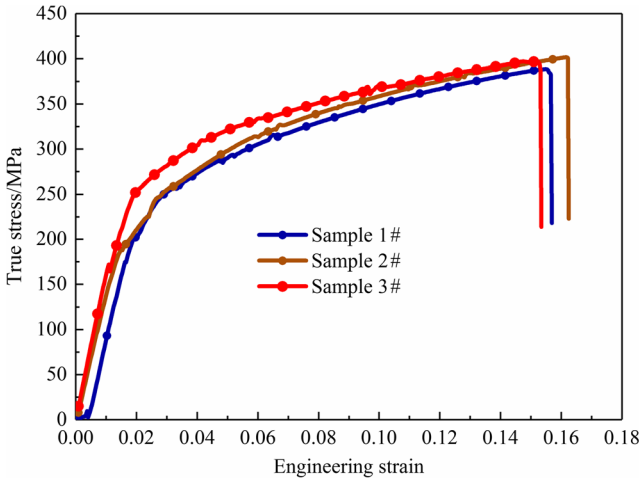

Fig. 14 Stress-strain curves of upper receiver forgings

Second, the microstructures coincide with the equivalent strain distribution obtained by the simulation results which are shown in Fig. 13. The effective strains of 1.5–2.5 located in position 5 are lower than those of 3–3.5 located in position 2. As expected, the mean grain size located in position 2 is finer than that located in position 5. The greater the effective strain, the finer the mean grain size.

The stress-strain curves of the upper receiver forgings are drawn in Fig. 14, in which three groups of samples of AZ80 magnesium alloy forgings treated by the second forging process have been measured in experiments. The values of the ultimate mechanical property are the average of the samples measured. Table 3 shows the tensile mechanical properties of the upper receiver forgings. The lateral and bottom ultimate tensile strengths are 406 and 396 MPa, respectively, and their elongations to fracture are 15 and 16%, respectively. The excellent mechanical properties in the final forgings are attributed to fine and equiaxed grains (Fig. 12). The main reason is

Table 3 Tensile mechanical properties of upper receiver forgings treated by the second forging process

Locations	Ultimate tensile strength (MPa)	Yield strength (MPa)	Elongation to fracture (%)
Lateral position	406	294	15
Bottom position	396	289	16

that grain boundaries are effective obstacles to dislocation motion, and small-grained materials will have a higher density of grain boundaries per unit volume. Moreover, a relatively low final forging temperature is helpful for reducing the softening effect caused by reheating. The slight differences of the mechanical properties between the lateral position and bottom position can also be attributed to the degree of deformation.

6 Conclusions

An isothermal closed-die forming process of a magnesium alloy upper receiver was conducted using the methods of numerical simulation and experiments, and the microstructure and mechanical properties of the upper receiver were analyzed comprehensively. The main conclusions are drawn as follows:

1. The two-stage hot precision forging process of the upper receiver, which was characterized by heading and final forging operations, has been developed according to the die filling status of extruded AZ80 magnesium alloy by adopting a 3D FE simulation.
2. The upper receiver forgings produced by the two-stage hot precision forging exhibit good qualities without any defects, such as under-filling and folds.
3. The forged piece has homogeneous microstructures, and the ultimate tensile strengths located in the lateral and bottom positions of forgings treated by two-stage forging are 406 and 396 MPa, respectively, and their elongations to fracture are 15 and 16%, respectively.

Acknowledgements This project is supported by National Natural Science Foundation of China (Grant No. 51822509).

References

1. Kulekci MK (2008) Magnesium and its alloys applications in automotive industry. Int J Adv Manuf Technol 39:851–865
2. Furuya H, Kogiso N, Matunaga S, Senda K (2000) Application pf magnesium alloys for aerospace structure systems. Mater Sci Forum 350-351:341–348
3. Lim SCV, Yong MS (2006) Plane-strain forging of wrought magnesium alloy AZ31. J Mater Process Technol 171(3):393–398
4. Skubisz P, Sińczak J, Bednarek S (2006) Forgeability of Mg–Al–Zn magnesium alloys in hot and warm closed die forging. J Mater Process Technol 177:210–213
5. Li F, Liu Y, Li XB (2017) Microstructure evolution and deformation behavior of AZ31 magnesium alloy during alternate forward extrusion. Acta Metall Sin (Engl Lett) 30(11):1135–1144
6. Jiang HW, Li F, Zeng X (2017) Microstructural characteristics and deformation of magnesium alloy AZ31 produced by continuous variable cross-section direct extrusion. J Mater Sci Technol 33(6): 573–579
7. Li F, Zeng X, Cao GJ (2015) Investigation of microstructure characteristics of the CVCDEed AZ31 magnesium alloy. Mater Sci Eng A 639:395–401
8. Ogawa N, Shiomi M, Osakada K (2002) Forming limit of magnesium alloy at elevated temperatures for precision forging. Int J Mach Tool Manu 42:607–614
9. Hsiang SH, Kuo JL (2005) Applying ANN to predict the forming load and mechanical property of magnesium alloy under hot extrusion. Int J Adv Manuf Technol 26:970–977
10. Li JQ, Liu J, Cui ZS (2015) Microstructures and mechanical properties of AZ61 magnesium alloy after isothermal multidirectional forging with increasing strain rate. Mater Sci Eng A 643:32–36
11. Kuo CC, Lin BT (2012) Optimization of springback for AZ31 magnesium alloy sheets in the L-bending process based on the Taguchi method. Int J Adv Manuf Technol 58:161–173
12. Li LL, Cai ZY, Xu HQ, Wang M, Yu J (2014) Research on AZ31 sheet one-pass hot spinning based on orthogonal experiment design. Int J Adv Manuf Technol 75:897–907
13. Wang Q, Zhang ZM, Zhang X, Yu JM (2008) Precision forging technologies for magnesium alloy bracket and wheel. Trans Nonferrous Metals Soc China 18:205–208
14. Karparvarfard SMH, Shaha SK, Behravesh SB, Jahed H, Williams BW (2017) Microstructure, texture and mechanical behavior characterization of hot forged cast ZK60 magnesium alloy. J Mater Sci Technol 33:907–918
15. Liu J, Cui ZS (2009) Hot forging process design and parameters determination of magnesium alloy AZ31B spur bevel gear. J Mater Process Technol 209:5871–5880
16. Hwang YM, Huang SJ, Huang YS (2013) Study of seamless tube extrusion of SiCp-reinforced AZ61 magnesium alloy composites. Int J Adv Manuf Technol 68(5–8):1361–1370
17. Xia XS, Xiao L, Chen Q, Li H, Tan YJ (2018) Hot forging process design, microstructure, and mechanical properties of cast Mg–Zn–Y–Zr magnesium alloy tank cover. Int J Adv Manuf Technol 94: 4199–4208
18. Shan D, Xu W, Han X, Huang X (2012) Study on isothermal precision forging process of rare earth intensifying magnesium alloy. Mater Sci Eng B 177:1698–1702
19. Cai Y, Sun CY, Wang WR, Li YL, Wan L, Qian LY (2018) An isothermal forming process with multi-stage variable speed for magnesium component assisted by sensitivity analysis. Mater Sci Eng A 729:9–20
20. Yuan L, Zhao Z, Shi WC, Xu FC, Shan DB (2015) Isothermal forming of the large-size AZ80A magnesium alloy forging with high mechanical properties. Int J Adv Manuf Technol 78:2037–2047
21. Lin P, Sun Y, Chi CZ, Wang WX (2017) Effect of plastic anisotropy of ZK60 magnesium alloy sheet on its forming characteristics during deep drawing process. Int J Adv Manuf Technol 88:1629–1637
22. Shan DB, Xu WC, Lu Y (2004) Study on precision forging technology for a complex-shaped light alloy forging. J Mater Process Technol 151:289–293
23. He HL, Huang SQ, Yi YP, Guo WF (2017) Simulation and experimental research on isothermal forging with semi-closed die and multi-stage-change speed of large AZ80 magnesium alloy support beam. J Mater Process Technol 246:198–204
24. Puchi-cabrera ES, Staia MH, Guérin JD, Lesage J, Dubar M, Chicot D (2013) Analysis of the work-hardening behavior of C-Mn steels deformed under hot-working conditions. Int J Plast 51(6):145–160
25. Hu FZ, Lin J, Chen W, Kang F, Hu CK, Huang SH, Chen Q (2016) Constitutive equation of 34Cr2Ni2Mo alloy structural steel for hot working. J Netshape Form Eng 8(6):1–6
26. Li WH, Dong XP, Chen XJ, Wu XQ (2010) Research and application of lubrication mechanism for aluminum alloy hot die forging. Forg Stamping Technol 35(3):128–131
27. Wen BC (2010) Handbook of mechanical design, 5th edn. Mechanical industry press, Beijing